

Structure formation in a colliding flow: the Herschel* view of the Draco Nebula

M.-A. Miville-Deschênes¹, Q. Salomé², P. G. Martin³, G. Joncas⁴, K. Blagrove³, K. Dassas¹, A. Abergel¹, A. Beelen¹,
F. Boulanger¹, G. Lagache⁵, F. J. Lockman⁶, and D. J. Marshall⁷

¹ Institut d'Astrophysique Spatiale, CNRS, Univ. Paris-Sud, Université Paris-Saclay, Bât. 121, 91405 Orsay cedex, France

² LERMA, Observatoire de Paris, CNRS UMR 8112, 61 avenue de l'Observatoire, 75014 Paris, France

³ Canadian Institute for Theoretical Astrophysics, University of Toronto, 60 St. George Street, Toronto, ON M5S 3H8, Canada

⁴ Département de physique, de génie physique et d'optique, Université Laval, Québec, QC G1V 0A6, Canada; Centre de Recherche en Astrophysique du Québec (CRAQ), Montréal, QC H3C 3J7, Canada

⁵ Aix-Marseille Université, CNRS, LAM (Laboratoire d'Astrophysique de Marseille) UMR 7326, 38 rue Frédéric Joliot-Curie, 13388, Marseille Cedex 13, France

⁶ National Radio Astronomy Observatory, P.O. Box 2, Rt. 28/92, Green Bank, WV 24944, USA

⁷ Laboratoire AIM, IRFU/Service d'Astrophysique - CEA/DSM - CNRS - Université Paris Diderot, Bât. 709, CEA-Saclay, 91191, Gif-sur-Yvette Cedex, France

March 26, 2022

ABSTRACT

Context. The Draco Nebula is a high Galactic latitude interstellar cloud observed at velocities corresponding to the Intermediate Velocity Cloud regime. It shows unusually strong CO emission and remarkably high-contrast small scale structures for such a diffuse high Galactic latitude cloud. Its 21 cm emission reveals that it is likely to have been formed by the collision of a Galactic halo cloud entering the disk of the Milky Way. Such physical conditions are ideal to study the formation of cold and dense gas in colliding flows of diffuse and warm gas.

Aims. The objective of this study is to better understand the process of structure formation in a colliding flow, as well as to describe the effects on the interstellar medium of matter from the Galactic halo that enters the disk.

Methods. To do so we have conducted *Herschel*-SPIRE observations of the Draco Nebula. The *clumpfind* algorithm was used to identify and characterize the small scale structures of the cloud.

Results. The high-resolution SPIRE map reveals the fragmented structure of the interface between the infalling cloud and the Galactic layer. This front is characterized by a Rayleigh-Taylor (RT) instability structure. From the determination of the typical length of the periodic structure (1.8 pc) we estimated the gas kinematic viscosity. This allowed us to estimate the dissipation scale of the warm neutral medium (0.1 pc) that was found to be compatible with that expected if ambipolar diffusion is the main mechanism of turbulent energy dissipation. The statistical properties of the small scale structures identified with *clumpfind* are found to be typical of that seen in molecular clouds and in hydrodynamical turbulence in general. The density of the gas has a log-normal distribution with an average value of 10^3 cm^{-3} . The typical size of the structures is 0.1-0.2 pc but this estimate is limited by the resolution of the observations. The mass of these structures ranges from 0.2 to $20 M_{\odot}$ and the distribution of the more massive ones follows a power law $dN/d \log(M) \sim M^{-1.6}$. We identify a mass-size relation with the same exponent as that found in giant molecular clouds ($M \sim L^{2.3}$). On the other hand we found that only 15% of the mass of the cloud is in gravitationally bound structures.

Conclusions. We conclude that the collision of diffuse gas from the Galactic halo with the diffuse interstellar medium of the outer layer of the disk is an efficient mechanism for producing dense structures. The increase of pressure induced by the collision is strong enough to trigger the formation of cold neutral medium out of the warm gas. It is likely that ambipolar diffusion is the mechanism dominating the turbulent energy dissipation. In that case the cold structures have sizes that are a few times the energy dissipation scale. The dense structures of Draco are the result of the interplay between magneto-hydrodynamical turbulence and the thermal instability as self-gravity is not dominating the dynamics. Interestingly they have properties typical of those found in more classical molecular clouds.

Key words. Turbulence - Methods:data analysis - Galaxy:halo - ISM:individual objects:Draco Nebula - ISM:kinematics and dynamics - ISM:structure

1. Introduction

One of the key questions regarding the formation of stars in galaxies is related to the way gas condenses, how it cycles from the hot and diffuse phase to cold and dense structures where stars form. This process is related to the formation of the Cold Neutral

Medium (CNM) and to the atomic-molecular (or H I-H₂) transition. One of the frameworks in which this general process is understood is related to colliding flows where a region of the Warm Neutral Medium (WNM) undergoes an increase of pressure that facilitates the rapid cooling of the gas to the stable CNM phase. This process has been studied in several numerical simulations (Hennebelle & Pérault 1999; Audit & Hennebelle 2005; Vázquez-Semadeni et al. 2006; Hennebelle et al. 2007; Inoue & Inutsuka 2009; Saury et al. 2014). One way of witnessing the

* *Herschel* is an ESA space observatory with science instruments provided by European-led Principal Investigator consortia and with important participation from NASA.

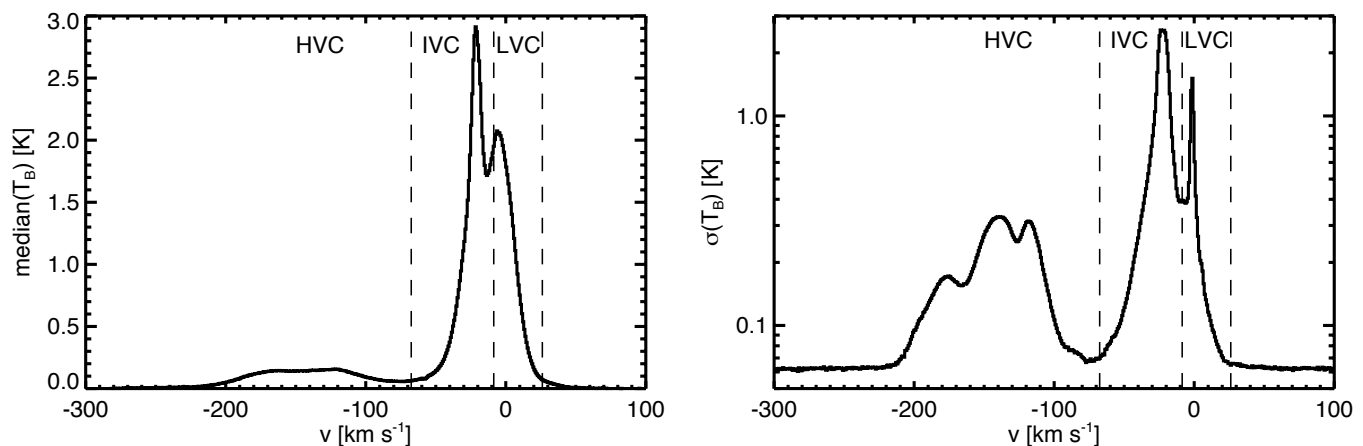


Fig. 1: Median (left) and standard deviation (right) spectra of the 21 cm emission in the Draco area. The GBT data used are from (Martin et al. 2015). The LVC, IVC and HVC velocity ranges are indicated by vertical dashed lines.

formation of cold structures in a colliding flow is by looking at the effects of Galactic halo clouds falling on the Milky Way disk.

Our Galaxy, as all galaxies, is an open and dynamical system. Matter is constantly arriving on the galactic disk. Part of this gas is the result of the galactic fountain: hot gas rises into the halo from stellar winds and supernovae then returns to the disk due to gravity (Shapiro & Field 1976; Bregman 1980; Putman et al. 2012). Matter also arrives from intergalactic space, either gas stripped from satellite galaxies or gas from the intergalactic medium (IGM). The origin of the material falling into the disk can partly be determined by its metallicity.

The high-velocity clouds (HVC) in our Galaxy are considered as possible direct evidence for extragalactic infalling gas. Measurements of the metallicity of HVC gas range from very low (0.1) up to solar (Collins et al. 2007). The intermediate-velocity clouds (IVC) are closer to the Galactic layer. Most of them are part of the Galactic fountain, but some should be matter of extragalactic origin that interacts with the disk. At this point it is unclear if the amount of new material entering the disk is sufficient to maintain the star-formation rate of galaxies (Peek et al. 2008; Sancisi et al. 2008).

This influx of matter from the halo is also adding kinetic energy to the interstellar medium (ISM). It is a way to input the supernovae energy into interstellar turbulence at some distance from where it was produced. One important question relates to the physical properties of the infalling gas and to the impact it has on the star formation cycle in galaxies (Heitsch & Putman 2009; Joung et al. 2012). Given the significant velocity (10s to 100s of km s^{-1}) with which matter encounters the Galactic disk, it is expected to be shocked and undergo dynamical instabilities. The thermal distribution of the gas, its density structure and the amount of molecular gas produced in the end is not well constrained observationally, partly due to the lack of observations that show this situation clearly.

The Draco Nebula (hereafter Draco), an icon among the IVCs, probably provides the best opportunity to understand these processes and resulting physical conditions. By chance there is little structured local ISM gas in the direction of Draco, allowing a very clear view at the matter entering the disk even in integrated (dust or gas) emission.

In this paper we complement what is already known about Draco by presenting *Herschel*-SPIRE (Griffin et al. 2010) maps of the nebula, revealing the fine details of its structure, especially

of its Rayleigh-Taylor front. We used these observations to quantify the typical length of the Rayleigh-Taylor instability, putting some constraints on the gas viscosity and the properties of turbulence in Draco. The high-resolution of the *Herschel*-SPIRE data also allows us to characterize the statistical properties of the small scale structures formed in the post-shock region, which enables us to quantify the outcome of the cloud collision in terms of structure formation.

The paper is organized as follows. In Sect. 2 we summarize what is known about Draco. Section 3 presents the data used for this study, how we computed the map of the column density and a description of the structure of the Rayleigh-Taylor instability front. The small scale structure is analyzed in Sect. 4. Our results are discussed in Sect. 5 and summarized in Sect. 6.

2. The Draco Nebula

2.1. A molecular intermediate velocity cloud

Draco is the most studied diffuse IVC at high Galactic latitude ($l \approx 91^\circ$, $b \approx 38^\circ$). It was first observed at 21 cm by Goerigk et al. (1983) at a velocity $v \sim -25 \text{ km s}^{-1}$, following on calibration observations obtained with the Effelsberg 100 m telescope (Kalberla et al. 1982). More recently, a $5^\circ \times 5^\circ$ region centered on Draco was observed at 21 cm with the Green Bank Telescope (GBT) as part of the GHIGLS survey (Martin et al. 2015). A smaller area was also covered at higher angular resolution with the interferometer of the Dominion Radio Astrophysical Observatory as part of the DHIGLS survey (Blagrove et al. 2016). In this region of the sky, three specific H I velocity components are seen: IVC, HVC and a low-velocity cloud, LVC, that corresponds to the gas in the solar neighbourhood. These three velocity components show up in the median and standard deviation 21 cm spectra (Fig. 1). Figure 2 presents their column density map based on the GHIGLS data.¹ These maps indicate that the H I column density in this direction of the sky is dominated by Draco, both in absolute value and in variations.

Goerigk et al. (1983) noticed that the H I cloud coincides with a faint optical nebula seen in the Palomar Observatory Sky Survey (POSS). They estimated that the ratio of dust extinction

¹ To identify the three components, we used the standard deviation spectrum of the 21 cm emission (Fig. 1 - right) following Planck Collaboration et al. (2011).

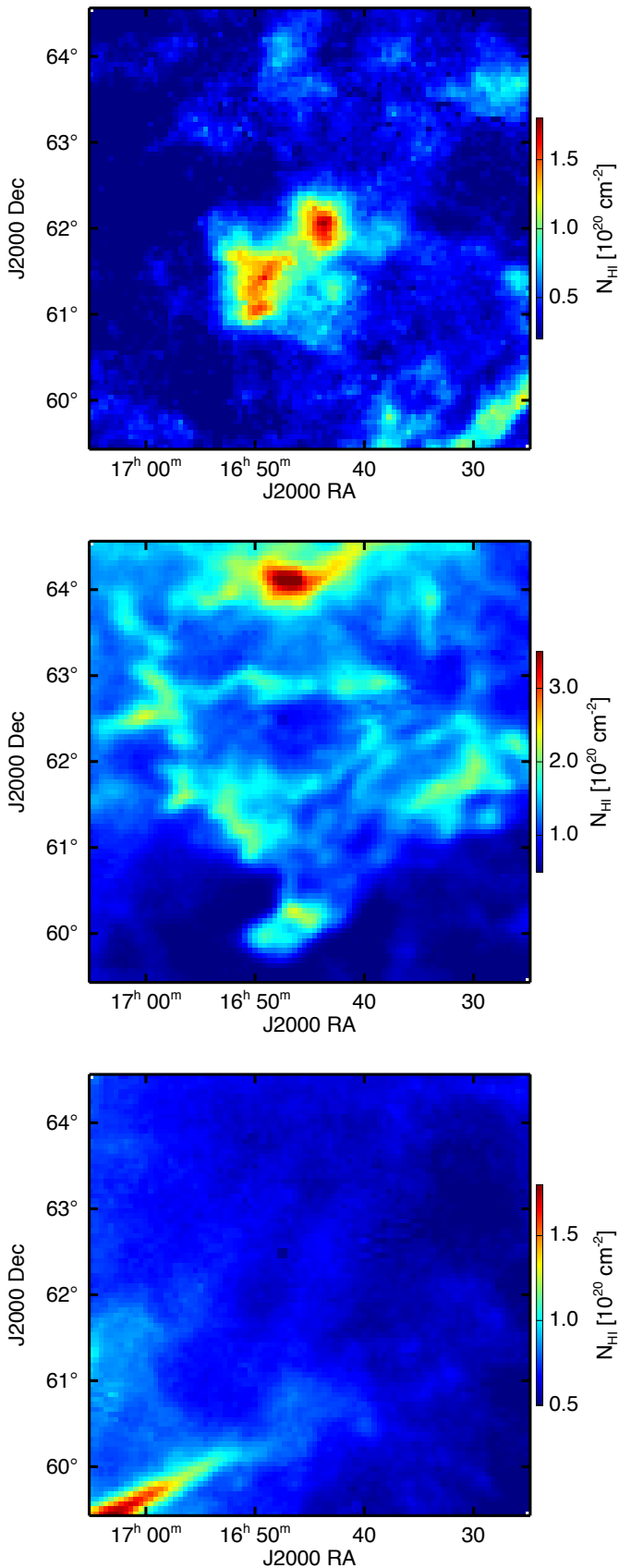


Fig. 2: H I column density maps in the direction of Draco for the LVC (bottom), IVC (middle) and HVC (top). Data were obtained at the Green Bank Telescope, they are part of the GHIGLS survey (Martin et al. 2015). The column density maps are the same as the ones used in Planck Collaboration et al. (2011).

to H I column density, N_{HI} , is unusually high, a factor 10 higher than typical values for diffuse clouds, which led them to conclude that most of the gas is in molecular form. From the analysis of their 21 cm data and its comparison with X-ray measurements, Goerigk et al. (1983) also suggested that Draco is the result of the interaction of Galactic halo gas entering the disk and that the details of its front-like structure is the result of the Rayleigh-Taylor (RT) instability.

The presence of molecular gas was attested by Mebold et al. (1985) and Rohlfs et al. (1989) who carried CO-observations of the brightest part of the nebula and found clumps of strong molecular emission at the boundary of the nebula. CO emission has also been detected by *Planck* (Planck Collaboration et al. 2014b). In addition, Stark et al. (1997) reported the detection of CH emission at 3.3 GHz and Park et al. (2009) presented far-UV observations showing the molecular hydrogen fluorescence over the whole Nebula.

Draco is part of the Magnani et al. (1985) catalog of high Galactic latitude molecular clouds (MBM 41 to 44). According to Magnani & Smith (2010) there are only five other regions at high Galactic latitude where intermediate velocity molecular gas (CO) has been detected, Draco being the one at the lowest Galactic latitude and the largest on the sky (about $4^\circ \times 4^\circ$).

Molecular gas was also revealed indirectly by X-ray data; Moritz et al. (1998) estimated that up to 70% of the hydrogen is molecular in the brightest parts of the nebula. Draco also appears as a shadow in the Soft X-ray ROSAT data, enabling to measure independently the column density of hydrogen (Burrows & Mendenhall 1991; Snowden et al. 1991). These measurements also imply that most of the gas is in molecular form. Similar conclusions are reached by comparing dust and 21 cm data (Herbstmeier et al. 1993; Planck Collaboration et al. 2011).

One specific feature of Draco is that it shows unusually strong CO emission for a diffuse cloud. It has significant CO emission on lines of sight where the total column density (derived either from dust emission or X-rays) is much lower than the usual threshold of $0.5 - 1 \times 10^{21} \text{ cm}^{-2}$ where molecular gas is usually seen in the ISM. In addition, large values of the ratio $W(^{12}\text{CO})/N(\text{H}_2)$ were deduced by Herbstmeier et al. (1993); Moritz et al. (1998). Also, Herbstmeier et al. (1994) observed higher CO transitions (up to $J=3-2$) to look for unusual excitation conditions but they found line ratios compatible with the average values found in cirrus clouds. This is indicative of a high CO abundance, potentially caused by an increase of the density due to the collision of a halo cloud entering the Milky Way disk.

2.2. Hot gas

There has been a few studies looking for hot gas in the area of Draco. Hirth et al. (1985) and Kerp et al. (1999) showed an excess of X-ray emission that seems to be spatially correlated with Complex C, but no clear relationship with Draco itself could be established. On the other hand, based on FUV observations, Park et al. (2009) reported the detection of several ionic lines in the direction of Draco, especially C IV, Si II and O III]. The C IV and Si II lines are seen outside Draco, possibly coming from the hot ionized Galactic layer. In addition, there is an excess of C IV, correlated with the dust emission of Draco. This excess is also seen in $H\alpha$ and O III], but not in Si II. Because of the absence of Si II, the authors concluded that the C IV, $H\alpha$ and O III] emission in Draco can not be the result of photo-ionization but it could be due to the radiative cooling of warm, shocked gas.

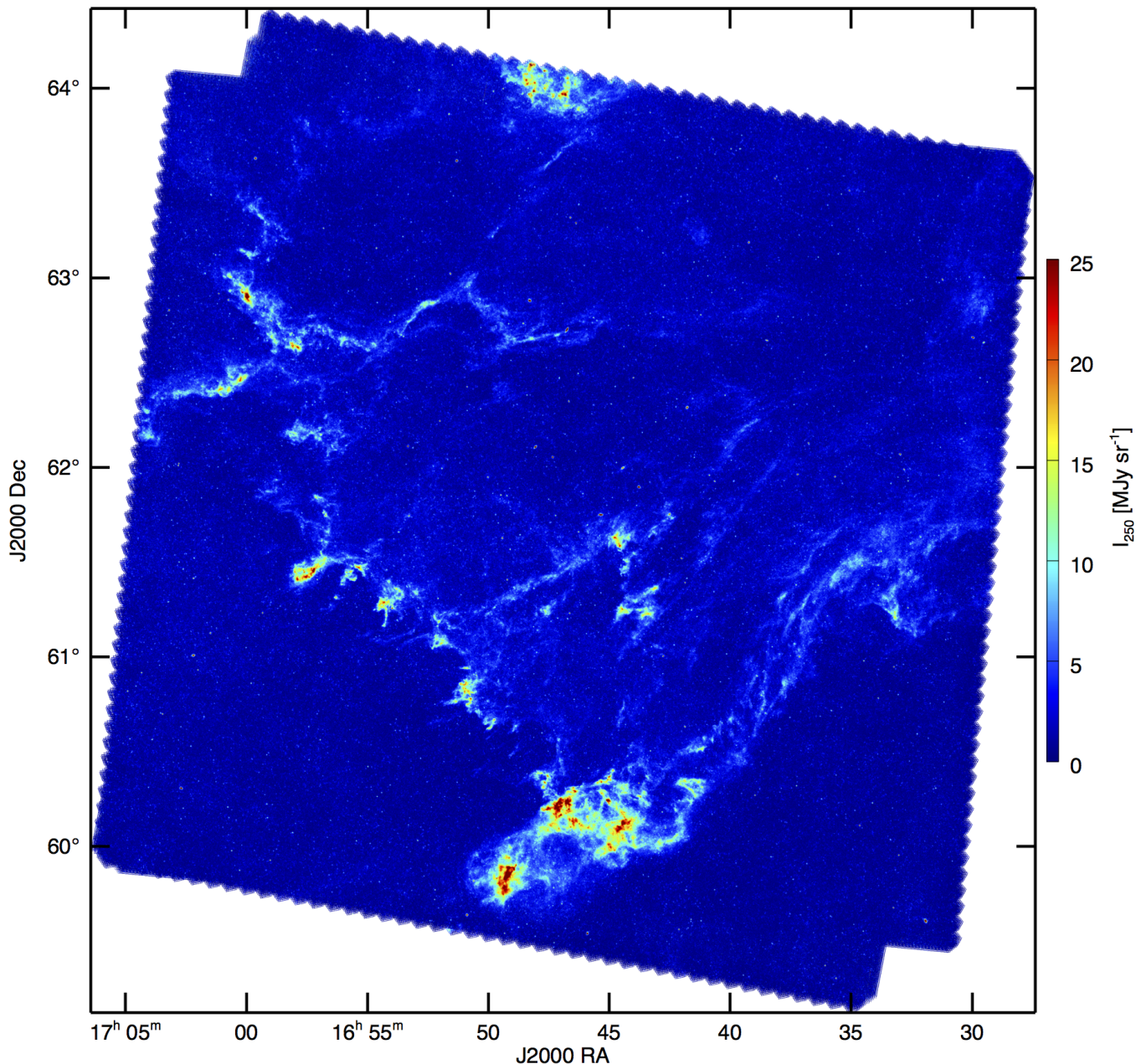


Fig. 3: The Draco Nebula at $250\mu\text{m}$ as observed with *Herschel*-SPIRE. From the comparison with *Planck* and H I data, the $250\mu\text{m}$ brightness is proportional to gas column density (see Section 3). The colorscale shown in this image translates to $0 < N_{\text{H}} < 6.2 \times 10^{21} \text{ cm}^{-2}$

2.3. Distance

An important clue informing any self-consistent description is the location of Draco in the Galaxy. Many attempts at estimating its distance have been made using different techniques. Star counts and color excess methods were used by Mebold et al. (1985); Goerigk & Mebold (1986); Penprase et al. (2000) giving distance estimates of $800 < d < 1300 \text{ pc}$. On the other hand, as pointed out by Lilienthal et al. (1991), both these methods have potential biases especially at low A_V . The only direct measure of the distance to Draco came from the detection of Na I D absorption lines at Draco’s systemic velocity in the spectrum of one star with known parallax distance (Gladders et al. 1998). Combined

with the non-detection for other foreground stars Gladders et al. (1998) estimated that $463_{-136}^{+192} \leq d \leq 618_{-174}^{+243} \text{ pc}$.

In the following, we adopt a distance of 600 pc. At the latitude of Draco, this distance corresponds to a height above the Galactic plane of $z = 370 \text{ pc}$. The half width at half maximum of the WNM in the Galactic disk being $\sim 265 \text{ pc}$; (Dickey & Lockman 1990), Draco is located in the upper part of the diffuse Galactic disk (or lower Galactic halo). What is clear is that Draco is out of the Local Bubble and so it must shadow X-rays coming from the Galactic halo.

The fact that Draco is located in the outer part of the Galactic disk is compatible with the fact that its brightness in the optical

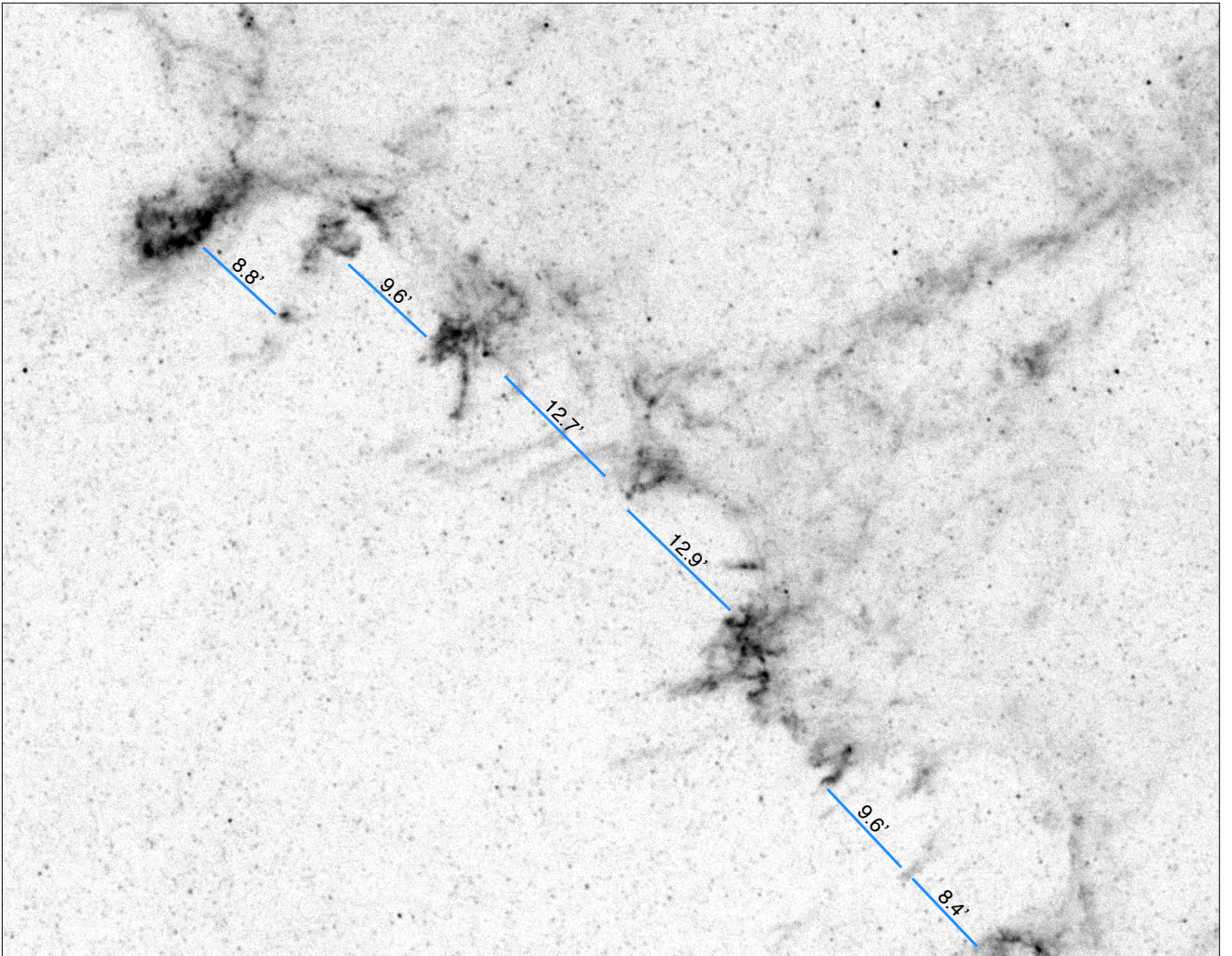


Fig. 4: Rayleigh-Taylor instability structure as seen in the $250\ \mu\text{m}$ SPIRE map. The blue lines give the apparent distance between fingers.

is comparable to clouds with dust properties typical of the disk (Mebold et al. 1985). It suggests that it is illuminated by a fairly standard interstellar radiation field and so is not likely to be located at kpc distances. A similar argument can be made from its infrared brightness.

3. *Herschel*-SPIRE map of Draco

Draco was observed with *Herschel* PACS (110 and $170\ \mu\text{m}$) and SPIRE (250, 350 and $500\ \mu\text{m}$) as part of the open-time program “*First steps toward star formation: unveiling the atomic to molecular transition in the diffuse interstellar medium*” (P.I. M-A Miville-Deschênes). A field of $3.85^\circ \times 3.85^\circ$ was observed in parallel mode. Unfortunately, an error occurred during the acquisition of the PACS data making them unusable. Therefore, the results presented here are solely based on SPIRE data, especially the $250\ \mu\text{m}$ map that has the highest angular resolution.

The SPIRE data were reduced using a standard procedure with HIPE v13. We used the product available on the HERSchel IdOc Database (HESIOD - <http://idoc-herschel.ias.u-psud.fr>). The zero level of each map was set by correlation with *Planck* data (see Sect. A). The SPIRE $250\ \mu\text{m}$ map of Draco is shown in Fig. 3. In what follows, we use the $250\ \mu\text{m}$ map converted to to-

tal hydrogen column density, N_{H} . The details of this conversion are given in Sect. A.

The *Herschel* data reveals for the first time the structure of matter in Draco at physical scales down to $0.05\ \text{pc}$ (resolution of $17.6''$ at $250\ \mu\text{m}$). The wispy and filamentary structure already seen in previous data (21 cm, far-infrared) is striking here. At the front structure at low declination where RT type structure were already identified, the SPIRE data reveals a wealth of clumpy structures organized in finger type structures.

One of the most striking features of the *Herschel* observations of Draco is the structure of the front that shows periodic half shells that are similar to structures produced by the Rayleigh-Taylor instability. A close-up view of the shock front is given in Fig. 4 revealing the typical arches. The size of the arches is variable, and the identification of the fingers is not always obvious. Nevertheless we found a variation of less than a factor of two with an average angular size of $10'.3$. Assuming a distance of $600\ \text{pc}$ and that the structures are orientated perpendicular to the line of sight, the typical length of the instability structure in Draco is $\lambda_{\text{max}} \approx 1.8\ \text{pc}$. In Sect. 5.2.1 we discuss on how this typical length might provide some information on the viscosity of the gas and on some properties of interstellar turbulence.

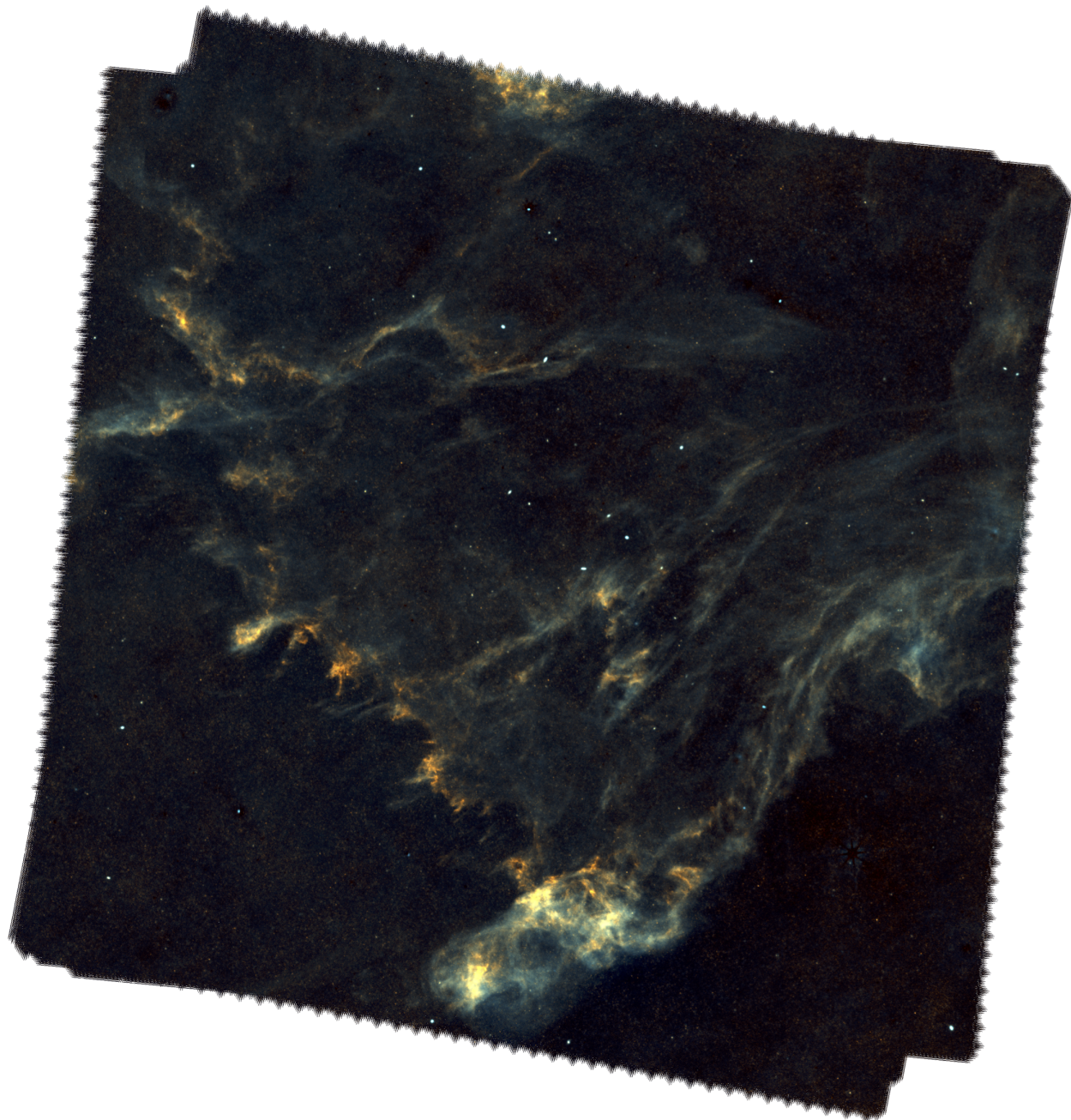


Fig. 5: The Draco Nebula. RGB image combining *Herschel*-SPIRE 250 μm (red) and WISE 12 μm (blue) from Meisner & Finkbeiner (2014). The green channel is the average of the two others. The size of the mosaic is $\sim 5^\circ \times 5^\circ$. The angular resolution of both maps is comparable (17.6'' for SPIRE 250 μm and 15'' for WISE 12 μm).

The 250 μm dust emission map reveals a higher dynamic range of the column density than 21 cm data. The H I column density (Fig. 2) ranges from 1 to $3 \times 10^{20} \text{ cm}^{-2}$ while the dust emission indicates a range from 3 to $50 \times 10^{20} \text{ cm}^{-2}$. It even reaches $N_{\text{H}} = 1 \times 10^{22} \text{ cm}^{-2}$ for a few pixels in the brightest parts in the southern region of the nebula. Part of this difference is due to different angular resolution of the GBT (9') and SPIRE (17.6'') data. Nevertheless, even when brought to the same angular resolution, a significant difference remains between the column density estimated with dust emission and 21 cm data. This confirms previous studies based on such comparison and that showed that a significant fraction of the bright region of Draco

is composed of molecular hydrogen (Herbstmeier et al. 1993; Planck Collaboration et al. 2011).

Figure 5 presents another view that combines SPIRE 250 μm and WISE 12 μm data (Meisner & Finkbeiner 2014). This image highlights strong variations of the relative abundance of smaller dust grains with respect to bigger ones. In particular, in the front-like structure, where strong CO emission is observed, there is almost no 12 μm emission, indicating a relative lack of smaller dust grains. One possibility is that smaller dust grains have disappeared, possibly through coagulation on bigger grains in a denser environment, similar to what is seen in molecular clouds. If that is the case, the colour variations in Fig. 5 could reflect somehow the variations of the gas density. Other possibilities

might relate back to the pre-existing grain populations in the WNM and their response to the collision.

4. Small scale structures

The *Herschel*-SPIRE data provide a striking view of the small scale structure of Draco (Figures 3, 4 and 5). In this section we characterize this structure and compare it with that seen in molecular clouds.

4.1. Structure identification

To characterize the general morphology of the nebula we broke it into individual structures using the 2D version of the *clumpfind* algorithm (Williams et al. 1994) that has been used extensively to identify structures in molecular clouds, in the Milky Way and external galaxies. Because it identifies islands above some brightness thresholds, *clumpfind* does not make any assumption on the shape or size of the structures. On the other hand, as it identifies structures using contours, *clumpfind* is rather sensitive to noise because it breaks contours at low brightness level.

When applied on the original $250\ \mu\text{m}$ map *clumpfind* identified only the brightest structures, leaving out more diffuse parts of the nebula that are visible by eye. To minimize the effect of noise clearly visible at the pixel size, we apply *clumpfind* on a version of the map convolved by a Gaussian kernel of $\text{FWHM}=30.5''$, to decrease the angular resolution by a factor of two, from $17.6''$ to $35.2''$. The smoothed map was then projected on a coarser grid with a pixel size twice the original size (from $6''$ to $12''$). The choice of the size of the smoothing kernel has no significant impact on the results presented here. The main goal here is to lower the noise level in the image analyzed by *clumpfind*.

We therefore applied *clumpfind* on the smoothed *Herschel*-SPIRE $250\ \mu\text{m}$ map, converted to N_{H} , with forty threshold values, equally spaced in log, from 1.25×10^{21} to $2.0 \times 10^{22}\ \text{cm}^{-2}$ (corresponding to 5 to $80\ \text{MJy sr}^{-1}$). The lowest threshold value is rather conservative but it rejects any contamination by galaxies while providing little impact on the properties of the identified structures.

The results do not depend significantly on the details of these choices. A total of 5028 structures were identified. Their properties are described next.

4.2. Physical properties

For each structure we defined a typical size, L , its mass, M , its density, n and its surface density, Σ . The histograms of these quantities are shown in Figs. 6 to 10.

4.2.1. Size of structures

For each structure identified we estimated a typical size, taking into account the brightness distribution of the structure. Each structure is composed of a number of pixels in the map, each pixel i defined by a position $[X_i, Y_i]$ and a column density $N_{\text{H},i}$. The structures are not assumed to be round; we estimate the length of their short and long axis using the inertia matrix (Saury et al. 2014)

$$M = \begin{bmatrix} \sigma^2(X) & \sigma^2(XY) \\ \sigma^2(XY) & \sigma^2(Y) \end{bmatrix} \quad (1)$$

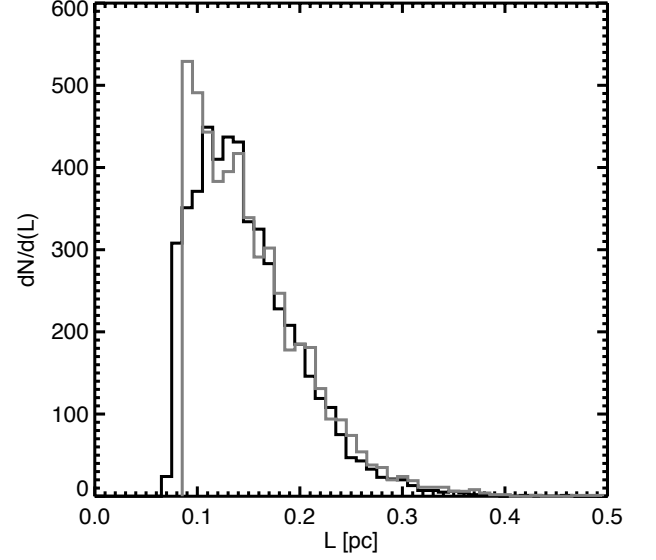


Fig. 6: Histogram of the size of each structure. The black line is the histogram of L computed using the eigenvalues of the inertia matrix. The grey line is the size defined as $R = \sqrt{A/\pi}$ where A is the area of each structure, proportional to the number of pixels.

where

$$\sigma^2(X) = \frac{1}{N_{\text{Htot}}} \sum_i N_{\text{H},i} (X_i - \langle X \rangle)^2 \quad (2)$$

$$\sigma^2(Y) = \frac{1}{N_{\text{Htot}}} \sum_i N_{\text{H},i} (Y_i - \langle Y \rangle)^2 \quad (3)$$

$$\sigma^2(XY) = \frac{1}{N_{\text{Htot}}} \sum_i N_{\text{H},i} (X_i - \langle X \rangle)(Y_i - \langle Y \rangle) \quad (4)$$

with

$$N_{\text{Htot}} = \sum_i N_{\text{H},i} \quad (5)$$

$$\langle X \rangle = \frac{1}{N_{\text{Htot}}} \sum_i N_{\text{H},i} X_i \quad (6)$$

$$\langle Y \rangle = \frac{1}{N_{\text{Htot}}} \sum_i N_{\text{H},i} Y_i. \quad (7)$$

The two eigenvalues of M correspond to the smallest and largest semi-axis of the structure, denoted respectively L_{min} and L_{max} . From them we define a typical size for the structure:

$$L = (L_{\text{max}} L_{\text{min}}^2)^{1/3}. \quad (8)$$

Here we make the hypothesis that an elongated structure projected on the sky is more likely to have a depth along the line of sight that corresponds to the smallest projected size on the sky.

We checked that for a uniformly weighted circle of radius R , this method gives $L = R$. More generally, L_{min} and L_{max}

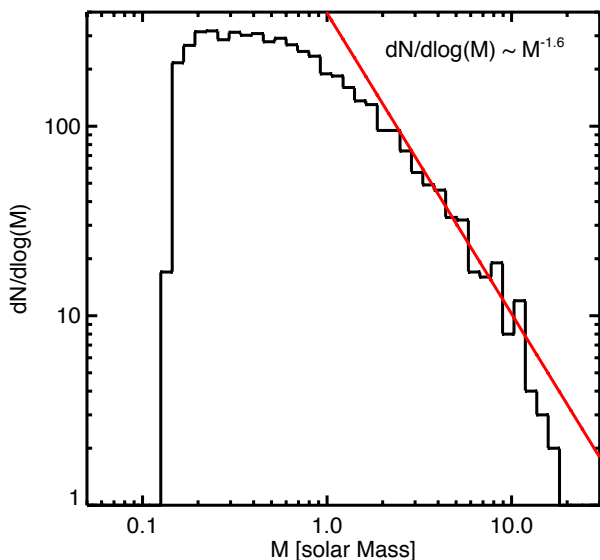


Fig. 7: $dN/d \log(M)$ diagram for the identified structures. The red line is a power law fit for range where $M \geq 3 M_{\odot}$.

correspond to the half length of an ellipse, whatever its orientation with respect to the $X - Y$ plane. For a point source with a Gaussian distribution of brightness of width σ , the typical size is $L = 1.77 \sigma$ or $L = 0.75 FWHM$.

At a distance of 600 pc, the angular resolution of the $250 \mu\text{m}$ map translates into a physical distance of 0.05 pc. This is the FWHM of the smallest structure that can be identified in the map. Our estimate of the size corresponds to $0.75 FWHM$ for a point like structure with a Gaussian shape, so the minimum value L can have is in fact 0.04 pc. By degrading the resolution of the original image by a factor of two, the minimum L is doubled to 0.08 pc. This corresponds exactly to the lowest value of L found here (see Fig. 6). The distribution of L has quite a narrow distribution; 50% of the structures have a size lower than twice the resolution ($L \leq 0.16$ pc) and 90% of them have a size lower than three times the resolution ($L \leq 0.24$ pc). The largest value of L is 0.47 pc.

We also considered another way of defining the size of a cloud using all the pixels detected, whatever the distribution of brightness. This approach is often used in the literature and in this case the typical size (or radius) of a cloud is defined as $R = \sqrt{A/\pi}$, where A is the surface of the structure (in pc^2), proportional to the number of pixels of the structure, N_{pix} . The histogram of R is also shown in Fig. 6 (grey line). Except for a slight difference at the smallest sizes (the minimum of R is 0.09 pc), these two methods give very concordant results. This is interesting because R is more sensitive to the noise level, or equivalently to the lowest contour level used to identify structures.

The fact that we are finding physical sizes that are similar to the resolution implies that the emission is varying strongly at small scales. This is compatible with the visual impression given by Figures 3, 5 and 4. The range of sizes found here is likely to be a combination of the angular resolution of the *Herschel*-SPIRE data and of how close small scale structures are. The size of a structure found by *clumpfind* is influenced by the distance to its neighbors. The fact that we find that 90% of the structures have a size lower than 0.25 pc is indicative that matter is structured significantly at scales smaller than that value.

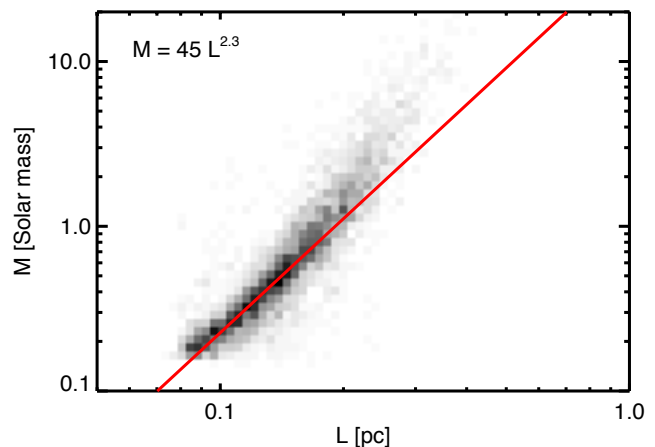


Fig. 8: Two-dimensional histogram of M versus L . The greyscale is proportional to the density of points. The red line is not a fit. It is indicative of the trend seen at low values of L and M .

4.2.2. Mass

The mass of each structure is defined as

$$M = N_{\text{Htot}} D^2 \tan^2(\delta) \mu m_{\text{H}} \quad (9)$$

where N_{Htot} is the total column density of a structure, summed over all pixels, D the distance, δ the pixel angular size and μ the molecular weight. Here we assumed $\mu = 1.4$ to take elements heavier than hydrogen into account.

The total amount of mass in the structures identified is $\sim 5.2 \times 10^3 M_{\odot}$. The mass distribution of the structures is shown in Fig. 7. The mass ranges from 0.1 to $20 M_{\odot}$ with a median value of $0.53 M_{\odot}$. We fitted the high mass part of the distribution using a power law $dN/d \log(M) \propto M^{-\alpha}$ assuming a $1/\sqrt{N}$ for each data point. The exact value of the power law exponent depends on the range over which the fit is performed. For $M \geq 3 M_{\odot}$ we obtain $\alpha = 1.6$. We noticed that the low end of the mass distribution has a shape similar to a log-normal distribution.

A mass distribution with a similar shape (log-normal plus power law tail) and a similar range in mass was found in a study of the core mass function (CMF) in Aquila by Könyves et al. (2010). These authors found that the high mass part of their $dN/d \log(M)$ is compatible with a power law with a slope of $\alpha = 1.5$. This is typical of that found for molecular clouds in general ($\alpha = 1.5 - 1.8$ for $M > 10^4 M_{\odot}$, Solomon et al. 1987; Kramer et al. 1998; Heyer et al. 2001; Marshall et al. 2009; Roman-Duval et al. 2010). These similarities are intriguing given the large difference in physical conditions between the cores of Aquila rift, the giant molecular clouds of the Milky Way and the clumps of Draco, and considering that different methods were used to identify structures. We note that similar slopes ($\alpha = 1.7 - 1.8$) are also found in various numerical simulations (Hennebelle & Falgarone 2012, and reference therein) done with different physical hypothesis, with and without gravity. This is indicative that the mass function is related to the nature of interstellar turbulence.

We note a general trend between the mass and size of the structures, similar to what is observed in more massive molecular clouds. Figure 8 shows a log-log density plot of the mass of the structures versus their size. The low end of the diagram is well modeled by a power law: $M = 45 L^{2.3}$, where L and M have units of pc and M_{\odot} respectively. On the other hand, the structures

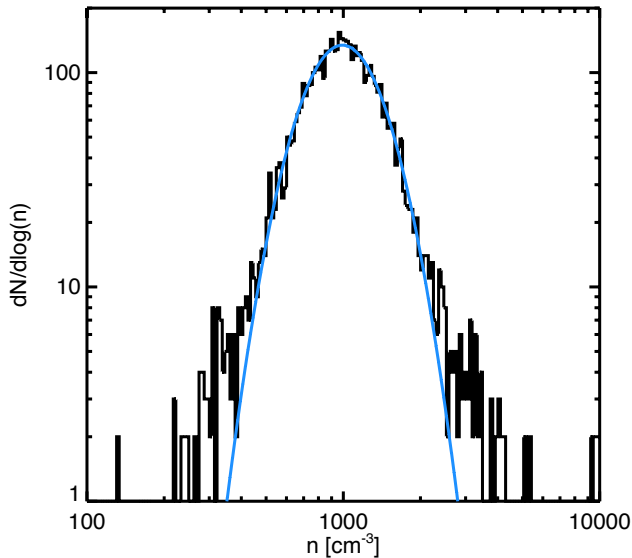


Fig. 9: $dN/d\log(n)$ diagram. The blue line is a log-normal fit of the distribution of the density n .

with sizes larger than 0.2 pc or masses larger than $1 M_{\odot}$ seem to depart from this relation; these structures are systematically more massive than what the relation predicts.

Several studies have highlighted such a relationship with a very similar exponent. Roman-Duval et al. (2010) found $M \propto r^{2.26}$ for molecular clouds having sizes in the range 0.7-30 pc. Heithausen et al. (1998) found $M \propto r^{2.31}$ for scales ranging from 0.01 to 1 pc. A similar mass-size relation is seen in numerical simulations where there is no gravity, and with or without heating and cooling processes included (Kritsuk et al. 2007; Federath et al. 2009; Audit & Hennebelle 2010). Because of the fact that this relation is seen in different physical condition, including isothermal gas, it is often attributed to turbulence.

4.2.3. Gas density

The gas density of each structure is defined by:

$$n = \frac{3M}{4\pi L^3 (\mu + f_{H_2}) m_H} \quad (10)$$

where $f_{H_2} = M_{H_2}/(M_{HI} + M_{H_2})$ is the fraction of the hydrogen that is in molecular form. It is expected that f_{H_2} varies across the Draco field; Herbstmeier et al. (1993) estimated that the molecular fraction varies from 0.04 to 0.7. The details of the H I-H₂ transition in Draco is beyond the scope of the present paper. Here we will assume a constant value of $f_{H_2} = 0.5$.

The histogram of n (Fig. 9) is very well represented by a log-normal distribution (i.e. $\log(n)$ is Gaussian distributed) with a median value of $1.0 \times 10^3 \text{ cm}^{-3}$ and a standard deviation of 0.14 in $\log_{10}(n)$. The density values given here assume that half of the hydrogen atoms are in H_2 . The majority of the structures have a density higher than the $^{12}\text{CO } J = 1 - 0$ critical density ($n(H_2) \sim 750 \text{ cm}^{-3}$).

The density found for GMCs is of the order $\langle n \rangle = 400 \pm 100 \text{ cm}^{-3}$ (Solomon et al. 1987; Roman-Duval et al. 2010). There is a general observed trend where smaller GMCs have

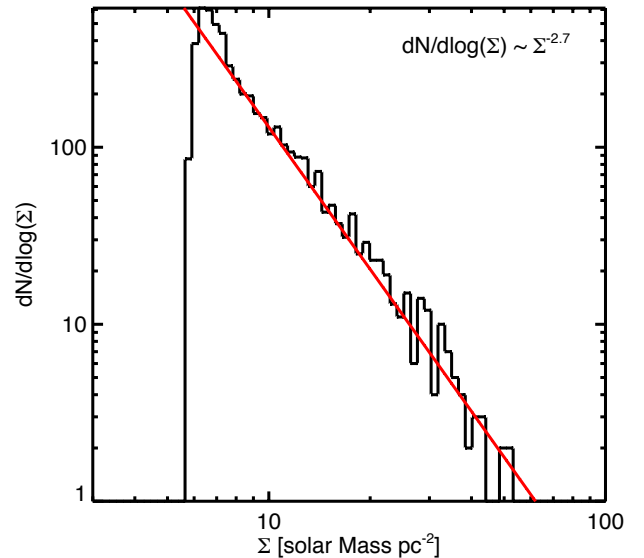


Fig. 10: $dN/d\log(\Sigma)$ diagram. The red line is a power law fit of the distribution.

higher densities.² For instance, from the sample of molecular clouds of (Roman-Duval et al. 2010), one obtains that $\langle n(H_2) \rangle = 800L^{-0.64}$. For the typical size of a structure in Draco ($L = 0.15 \text{ pc}$, see Fig. 6) that relationship would predict $\langle n(H_2) \rangle = 2.7 \times 10^3 \text{ cm}^{-3}$, only a factor of 3 more than what we estimated. Given the large dispersion of the $n_{H_2} - L$ relation observed in the ISM, the values obtained here seem typical for molecular clouds.

4.2.4. Surface density

By definition the surface density is $\Sigma = M/A$ where A is the surface of the cloud on the sky, expressed in pc^2 . Therefore Σ has units of $M_{\odot} \text{ pc}^{-2}$. Nevertheless this quantity is in fact independent of distance. The surface density of clouds depends significantly on how clouds are identified and on the noise level of the observations. Solomon et al. (1987) and Roman-Duval et al. (2010) found $\Sigma \sim 140 - 200 M_{\odot} \text{ pc}^{-2}$ but, using higher angular resolution data and a different tracer (^{13}CO instead ^{12}CO) Heyer et al. (2009) reported a median of $\Sigma = 42 M_{\odot} \text{ pc}^{-2}$.

Interestingly, for Draco the distribution of Σ (Fig. 10) follows a power law: $N(\Sigma) \propto \Sigma^{-2.8}$ for the whole range of values found here, from 6 to $60 M_{\odot} \text{ pc}^{-2}$. The median value of our sample is $7.6 M_{\odot} \text{ pc}^{-2}$, much below what is usually seen in molecular clouds.

4.2.5. Jeans mass

To evaluate the gravitational stability of the structures in Draco we compared their mass with the Jeans mass that gives the maximal mass of a stable isolated and spherical clouds (Lequeux

² This is related to the very clumpy and open structure of molecular clouds which implies a volume filling factor lower than unity. In other words, the mass does not scale with L^3 (see Fig. 8), therefore the density estimated over large physical scales is an underestimate of the density at small scales, explaining why the average density in GMCs is found to be smaller than the critical density of CO.

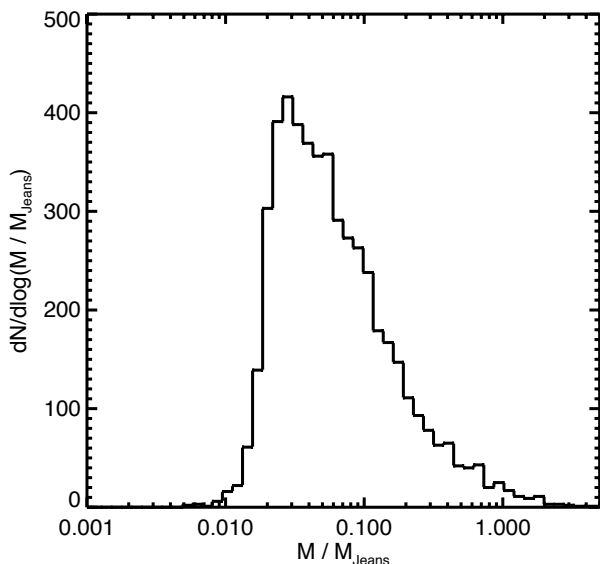


Fig. 11: $dN/d\log(M/M_{\text{Jeans}})$ diagram.

2005):

$$M_j = \left(\frac{1}{\mu m_H}\right)^2 \left(\frac{5 kT}{2 G}\right)^{3/2} \left(\frac{4}{3} \pi n\right)^{-1/2} \quad (11)$$

where μ is the molecular weight (equals to 1.4 or 2.4 for fully atomic or molecular hydrogen respectively).

Only 1% of the structures have a mass larger than the Jeans mass (Fig. 11). These structures are the more massive. They encompass 15% of the total mass of the structure identified.

5. Discussion

The *Herschel*-SPIRE observations of Draco reveal two important aspects of the gas structure resulting from the collisions of two flows. The observations reveal a dense front with regularly spaced fingers of dense gas, a structure typical of the RT instability, as well as numerous and contrasted small scale structures (clumps).

5.1. Formation scenario

According to what was proposed very early on (Kalberla et al. 1984; Mebold et al. 1989; Rohlfs et al. 1989), Draco seems to be the result of the compression of warm gas in the outer part of the Galactic WNM layer ($z \sim 370$ pc) due to the collision with a cloud falling from the Galactic halo.

There has been some speculation about the potential role of the HVC component seen at $v_{\text{LSR}} \sim -150 \text{ km s}^{-1}$ in the formation of Draco (Hirth et al. 1985). The morphology of the three H I components (Fig. 2) could suggest that the IVC (Draco) is the result of the dynamical interaction between the HVC and the LVC. Along those lines, Pietz et al. (1996) proposed that faint 21 cm emission at velocities between the HVC and the IVC could be due to an inelastic collision of HVC gas with the Galactic thick disk. This emission is extremely faint (see Fig. 1) and the dynamical picture that would physically link the HVC and IVC components is unclear to us. We rather favour a scenario where the observed HVC is not directly involved in the formation of Draco.

Benjamin & Danly (1997) suggested that IVCs and HVCs have trajectories in the Galactic halo compatible with clouds falling on the Galactic disk, attracted by the Milky Way gravitational potential and slowed down by their interaction with the Galactic ISM. In this scenario, IVCs and HVCs would have reached their terminal velocity. They stressed this picture is compatible with the observations as clouds closer to the plane have lower absolute velocity than clouds far away.³ Draco fits that picture: given its column density and height above the plane, its observed velocity ($v = v_{\text{LSR}}/\sin b = 40 \text{ km s}^{-1}$) is comparable to its expected terminal velocity ($v_t \approx 50 \text{ km s}^{-1}$, see Sect. B and Benjamin 1999).

If Draco has indeed reached its terminal velocity, its average velocity does not inform us on its origin (Galactic fountain or extragalactic gas). It could have once been an HVC but it would have slowed down as it interacted with the ISM of the disk. One fact that could favor the Galactic fountain origin is the bright dust and CO emission, showing that it contains a significant amount of heavy elements. On the other hand, the matter that composes Draco today could be Galactic gas swept up by an originally low metallicity cloud that has been slowed down by the Galactic ISM. At $z = 370$ pc above the Galactic plane, the total column density ($\text{H I} + \text{H}^+$) encountered by a cloud coming from infinity is about $N_{\text{H}} = 1 \times 10^{20} \text{ cm}^{-2}$ (Sect. B). This is similar to the column density of Draco itself. Therefore, a large fraction of the mass of Draco could be composed of Galactic gas with near solar metallicity. A detailed study of the metallicity of the gas in Draco could provide some answers to that question.

Whatever the origin and metallicity of the infalling cloud, it seems likely that it has accelerated and pressurized WNM gas at rest in the Galactic layer, producing a shocked front of denser gas that is progressing towards us in the diffuse ISM. The structure of Draco itself, with its long cometary plumes, is indeed reminiscent of a dense cloud moving in a more diffuse medium (Odenwald & Rickard 1987). The structure of the front, with its sharp increase in column density, is also indicative of a shock. Assuming $T = 8000 \text{ K}$ and taking elements heavier than hydrogen into account, Draco moves with respect to the Galactic ISM with a Mach number of $M = 5.8$. This scenario is compatible with the FUV observations of Park et al. (2009) that show the presence of hot gas due to shock heating. In addition, these conditions are favourable for the development of a RT instability at the interface, as well as for the formation of CNM out of compressed WNM through the thermal instability (Saury et al. 2014).

5.2. Turbulence

In this section we use the RT typical length, combined with velocity information from the 21 cm data, to estimate parameters of interstellar turbulence like the rate of transferred energy, ϵ , the Reynolds number, Re , and the turbulence dissipation scale, l_d . The values of these parameters estimated for Draco are summarized in Table 1.

5.2.1. Rayleigh-Taylor instability and gas viscosity

The RT instability occurs when two fluids are accelerated towards each other. For the incompressible case, the fluids cannot interpenetrate freely, bubbles of the light fluid rise into the heavy fluid forming finger structures. It appears that such structures are

³ obviously, in the case where only gravity is taken into consideration, clouds would accelerate continuously and cross the disk at high speed.

also observed in compressible fluids, like supernovae remnants (Ellinger et al. 2012). In our case, the fingers are pointing towards the Galactic plane, indicating that Draco is denser than the medium in which it is moving towards, i.e., the Galactic WNM layer.

For two incompressible fluids of constant viscosity separated by a horizontal boundary, Chandrasekhar (1961) showed that the RT instability typical length is given by:

$$\lambda_{\max} = 4\pi \left(\frac{v_{\text{kin}}^2 A}{a} \right)^{1/3} \quad (12)$$

where v_{kin} is the kinematic viscosity, a is the acceleration, and

$$A = \frac{\rho_1 - \rho_2}{\rho_1 + \rho_2} \quad (13)$$

is the Atwood number that takes values between 0 and 1. Here ρ_1 and ρ_2 are the density of the heavier and lighter fluids respectively.

Chandrasekhar's study of hydrodynamic stability was made for incompressible fluids which is not the case in the interstellar medium. However, Ribeyre et al. (2004) studied the compressible case for supernovae and concluded that compressibility slows down the growth of the RT instability but it has no important impact on λ_{\max} . The typical length of the RT instability in supernovae is usually estimated with equation 12 (Ellinger et al. 2012). The same assumption will be made here. Interestingly, Eq. 12 offers us the opportunity to estimate the gas viscosity knowing the instability typical length, the gas acceleration and A .

What acceleration should be considered here? In the classical picture of two fluids, one on top of the other, a is the gravitational acceleration. Here the gas is slowed down by the friction with the Galactic ISM. In fact the cloud is decelerating as it gets closer to the disk, slowly reaching $v = 0$. Assuming that Draco has reached its terminal velocity, we estimated that its deceleration is $a = 2.3 \times 10^{-8} \text{ cm s}^{-2}$ (see Sect. B).

The parameter A depends on the density of the two fluids. The density of the gas at a height above the plane of $z \approx 370 \text{ pc}$, the assumed location of Draco, is $n = 0.07 \text{ cm}^{-3}$ (see Sect. B). For Draco, the density can be estimated using the dust emission and 21 cm data. The gas column density, averaged over the whole nebula, is about $1.3 \times 10^{20} \text{ cm}^{-2}$. Draco spans about 3° on the sky, which translates into 30 pc at a distance of 600 pc. Assuming a depth of 30 pc for the infalling cloud, its average density would be of the order of 1.4 cm^{-3} . This is an averaged value that represents the density of the WNM in Draco. The density is certainly larger at the shock front where strong CO emission (as well as CH, Stark et al. 1997) is observed (the CO critical density is of the order of 10^3 cm^{-3}). Assuming $n_1 = 1.4 \text{ cm}^{-3}$ and $n_2 = 0.07 \text{ cm}^{-3}$, the Atwood number is $A = 0.90$. Using Eq. 12, the kinematic viscosity is $v_{\text{kin}} = 4.7 \times 10^{22} \text{ cm}^2 \text{ s}^{-1}$.

It is interesting to compare v_{kin} to the more classical molecular viscosity

$$v_{\text{mol}} = \frac{1}{3} \frac{1}{\sigma n} \sqrt{\frac{3 kT}{2 \mu m_{\text{H}}}} \quad (14)$$

For typical values of temperature and density for the WNM in Draco ($T = 8000 \text{ K}$, $n = 1.4 \text{ cm}^{-3}$) and assuming $\sigma = 1 \times 10^{-15} \text{ cm}^{-2}$ for the hydrogen cross-section (Lequeux 2005), the molecular viscosity is $v_{\text{mol}} = 2.0 \times 10^{20} \text{ cm}^2 \text{ s}^{-1}$.⁴ This is more

⁴ The molecular viscosity of the CNM is even smaller: $v_{\text{mol}} = 1.0 \times 10^{18} \text{ cm}^2 \text{ s}^{-1}$ assuming $T = 100 \text{ K}$ and $n = 30 \text{ cm}^{-3}$.

Table 1: Properties of the turbulence in Draco.

Quantity	Symbol	Value	Units
Largest scale	L	30	pc
Average velocity	\bar{v}_l	11.2	km s^{-1}
Rayleigh-Taylor length	λ_{\max}	1.8	pc
Viscosity	v_{kin}	4.7×10^{22}	$\text{cm}^2 \text{ s}^{-1}$
Reynolds number	Re	2100	
Energy transfer rate	ϵ	7.6×10^{-3}	$L_\odot M_\odot^{-1}$
Dissipation scale	l_d	0.1	pc

than 200 times smaller than what is estimated using the RT typical length and Eq. 12. That results depends on the distance to the power 3/2. Even if we assumed a distance to Draco of 400 pc, the kinematic viscosity would still be more than 150 times larger than the molecular viscosity.

5.2.2. Energy transfer rate

An important parameter that characterizes the turbulent cascade of energy is the energy transfer rate by unit of mass,

$$\epsilon = \frac{1}{2} \frac{\bar{v}_l^3}{l} \quad (15)$$

Here l and \bar{v}_l represent the typical scale and the typical average velocity of the flow. We assumed $l \sim 30 \text{ pc}$ for the largest scale of the flow. The average velocity of the gas at that scale is best estimated by looking at the width of the 21 cm line, averaged over the whole region. Using the 21 cm GBT data (Fig. 2) we estimated the velocity dispersion of the IVC component to be $\sigma_v = 10.7 \text{ km s}^{-1}$, which is likely to be dominated by the warm phase. Removing the thermal contribution to the linewidth (assuming $T = 8000 \text{ K}$), this reduces to $\sigma_v = 7.0 \text{ km s}^{-1}$. Assuming a Gaussian distribution of velocity, this corresponds to an average velocity of $\bar{v}_l = \sqrt{8/\pi} \sigma_v = 11.2 \text{ km s}^{-1}$.

The energy transfer rate of the WNM in Draco is $\epsilon = 7.6 \times 10^{-3} L_\odot M_\odot^{-1}$. This value is slightly higher than that estimated for the H I in the Solar neighborhood ($\epsilon \sim 10^{-3} L_\odot M_\odot^{-1}$, Hennebelle & Falgarone 2012).

5.2.3. Reynolds number

By combining velocity information from the 21 cm data with the measurement of v_{kin} , one can estimate the Reynolds number of the flow

$$Re = \frac{l \bar{v}_l}{v_{\text{kin}}} \quad (16)$$

For Draco, we find $Re = 2100$, a value significantly smaller than the more traditional estimates for the ISM ($Re \sim 10^5$, Chandrasekhar 1949). This difference is explained by the fact that $v_{\text{kin}} \gg v_{\text{mol}}$ as Re is usually computed assuming that the dissipation of turbulent energy is dominated by molecular viscosity.

5.2.4. Dissipation scale

Turbulent energy in the ISM is dissipated via either viscous (hydrodynamical) or resistive (MHD) processes, depending on

which process happens at the largest scale (Benjamin 1999; Hennebelle & André 2013). The scale at which turbulent energy is dissipated is

$$l_d \approx \left(\frac{v^3}{\epsilon} \right)^{1/4}. \quad (17)$$

Like for Re , the scale at which turbulent energy is dissipated depends on what process is more efficient at transforming motion into heat. Assuming that $\nu = \nu_{\text{kin}}$, the dissipation scale is $l_d = 0.1$ pc. This is close to two to three orders of magnitude larger than what is generally estimated for the WNM ($l_d \sim 0.003$ pc) and the CNM ($l_d \sim 2$ AU) assuming that the dissipative process is molecular viscosity (Lequeux 2005).

The other potential dissipative process is the ion-neutral friction. Following Lequeux (2005), the ambipolar diffusion typical scale is

$$l_{\text{AD}} = \sqrt{\frac{\pi}{\mu m_{\text{H}} 2X \langle \sigma v \rangle n_n^{3/2}}} B \quad (18)$$

where X is the ionization fraction, n_n the density of neutrals, and $\langle \sigma v \rangle$ the collision rate between ions and neutral (assumed to be the Langevin rate $2 \times 10^{-9} \text{ cm}^3 \text{ s}^{-1}$). For typical conditions in the ISM, from warm gas to molecular clouds, l_{AD} is often larger than the dissipation scale for molecular viscosity. It is the case in Draco; assuming $n_n = 1.4 \text{ cm}^{-3}$ (the density of the compressed WNM) and $B = 6 \mu\text{G}$, a typical value for the WNM in the solar neighborhood (Beck 2001), the ambipolar diffusion scale is also $l_{\text{AD}} = 0.1$ pc.

The kinematic viscosity estimated from the RT-like structures indicates that the dissipation of energy happens at a scale of ~ 0.1 pc, much larger than the dissipation scale of molecular viscosity but in agreement with what is expected if ambipolar diffusion is the dominant process of energy dissipation.

5.2.5. Wardle instability

Given that the magnetic field seems to play an important role in the dynamics, one could consider that the structure of the front is the result of the Wardle instability (Wardle 1990). This instability occurs due to the velocity difference between neutrals and ions, when the Alfvén Mach number, M_A , is greater than 5. The Alfvén speed in a WNM with $n = 0.1 \text{ cm}^{-3}$ and $B = 6 \mu\text{G}$ is $V_A = 35.0 \text{ km s}^{-1}$. Considering that the velocity of the shock is 40 km s^{-1} , the Alfvén Mach number is $M_A = 1.1$. This suggests that the Wardle instability is not dominant in Draco.

5.3. Dense structures

Using the two-dimension version of *clumpfind* on the *Herschel*-SPIRE 250 μm , converted to N_{H} , structures of sizes from 0.08 to 0.5 pc were revealed. Interestingly, these small structures share many properties with much more massive molecular clouds as well as with prestellar cores. First, the mass distribution ranging from 0.1 to $20 M_{\odot}$ with a median value of $0.53 M_{\odot}$ is very similar to a prestellar cores mass distribution (Könyves et al. 2010). In addition, the mass-size relation ($M \propto L^{2.3}$) and the mass histogram ($dN/d \log(M) \propto M^{-1.6}$) are typical of that seen in more massive molecular clouds.

On the other hand, unlike prestellar cores (Könyves et al. 2010) and unlike molecular clouds (Roman-Duval et al. 2010), 85% of the structures found in Draco are not gravitationally

bound. This is compatible with the fact that the density histogram is found to be log-normal, something generally associated with compressive supersonic flows without gravity (Kritsuk et al. 2007). We also note that the density of the structures in Draco, even though they are large enough ($n \sim 1000 \text{ cm}^{-3}$) to explain the strong CO emission observed, are 100 times less than that seen in prestellar cores.

We suggest that the formation of dense structures seen in Draco is the result of the transition from the WNM to cold and dense gas through the thermal instability of H I. This transition is favored by the compression of the warm gas at the interface between the Galactic layer and the infalling matter. As shown in several numerical simulations, the increase of density of the WNM sends the gas in a thermally unstable state that favors the transition to the CNM (Hennebelle & Pérault 1999; Audit & Hennebelle 2005; Vázquez-Semadeni et al. 2006; Inoue & Inutsuka 2009; Saury et al. 2014). If the increase in density is sufficient, the formation of molecules is expected; using hydrodynamic simulations of a strong shock wave propagating into WNM, Koyama & Inutsuka (2000) showed that it can produce a thin and dense H_2 layer via thermal instability. They also predict fragmentation of the thermally collapsed layer into small molecular structures, similar to that seen in Draco.

The fact that the CMF and molecular clouds mass spectrum have a similar power law index has been used as an argument in favor of turbulence as being responsible for the fragmentation and structuration of matter in dense environments. On the other hand because of the fact that most of these objects are gravitationally bound, it is difficult to exclude the role of gravity, even though numerical simulations without gravity tend to obtain similar mass spectra. In this context, Draco is interesting as it reveals a clear example of dense structures, formed through hydrodynamical processes combined with the thermal instability of H I, with the exact same statistical properties as gravitationally bound systems.

The small scale structures of Draco have sizes slightly larger (0.1 to 0.5 pc) than the WNM dissipation scale estimated here ($l_d = 0.1$ pc). In addition they have statistical properties of a turbulent flow. Numerical simulations (e.g., Saury et al. 2014) have shown that the formation of CNM structures happens when the WNM is thermally unstable (i.e., compressed) and if the cooling time is shorter than the dynamical time. These two conditions must be satisfied in order for the transition to occur. The cloud collision provides the necessary increase in WNM density but at the same time, the input of kinetic energy increases the amplitude of the turbulent motions (as attested by the value of ϵ slightly higher than what is seen in the Solar neighborhood), lowering the dynamical time. The formation of CNM can then only occur if a fraction of the turbulent energy is dissipated such that dynamical time becomes lower than the cooling time. We propose that the dissipation of turbulent energy of the WNM via the ambipolar diffusion, provides favourable conditions for the formation of dense structures at scales close to l_d .

6. Conclusion

We presented *Herschel*-SPIRE observations of the Draco Nebula, a diffuse high Galactic latitude interstellar cloud located about 370 pc above the Galactic plane. Draco is likely to be the result of the compression of diffuse gas of the outer WNM layer by the collision of a cloud falling from the Galactic halo. It offers a unique opportunity to study the formation of dense structures in a colliding flow.

The *Herschel* data reveal the fine details of the structure of this cloud, especially of a front that shows a typical Rayleigh-Taylor instability structure. From the typical length of this structure we were able to estimate the gas kinematic viscosity. Combined with 21 cmGBT data, we estimated the Reynolds number ($Re = 2100$), the energy transfer rate ($\epsilon = 7.6 \times 10^{-3} L_{\odot} M_{\odot}^{-1}$) and the dissipation scale of the turbulent cascade ($l_d = 0.1$ pc). The viscosity and dissipation scale are typical of values that would be found in the WNM in the case that the turbulent energy dissipation is dominated by ambipolar diffusion.

The SPIRE 250 μm map reveals high contrast structures with a wealth of small scale clumps. Using the *clumpfind* algorithm, a total of 5028 structures were identified, with physical sizes ranging from 0.08 to 0.5 pc, the lower limit being set by the angular resolution of the data. The mass spectrum is very close to that of prestellar cores (in terms of shape and range), even though the densities in Draco are 100 times lower. The high mass part of the mass spectrum is well represented by a power law $dN/d \log(M) \propto M^{-1.6}$, like that seen for prestellar cores and molecular clouds. On the other hand, the majority of the structures (85% in mass) are not gravitationally bound. This is corroborated by the fact that the density spectrum clearly follows a log-normal distribution.

The results presented here reveal dense structures formed in a colliding flow where gravity is not a dominant process. We showed that these structures are likely to be the result of the transition from the WNM to CNM through the H I thermal instability. We propose that the formation of dense structures is favoured by the dissipation of the turbulent energy in the WNM through ambipolar diffusion, at a scale of $l_{AD} = 0.1$ pc. The energy dissipation favours the formation of small CNM structures at scales slightly larger than l_{AD} . The fact that these structures share many statistical properties with denser environments is an indication of the importance of interstellar turbulence and the thermal instability in shaping the structure of star-forming regions

Acknowledgements. Herschel-SPIRE has been developed by a consortium of institutes led by Cardiff University (UK) and including Univ. Lethbridge (Canada); NAOC (China); CEA, LAM (France); IFSI, Univ. Padua (Italy); IAC (Spain); Stockholm Observatory (Sweden); Imperial College London, RAL, UCL-MSSL, UKATC, Univ. Sussex (UK); and Caltech, JPL, NHSC, Univ. Colorado (USA). This development has been supported by national funding agencies: CSA (Canada); NAOC (China); CEA, CNES, CNRS (France); ASI (Italy); MCINN (Spain); SNSB (Sweden); STFC, UKSA (UK); and NASA (USA).

Appendix A: Estimating Gas column density from dust emission

Here we are interested in using the large dust grain emission as a tracer of column density. To do so, it is customary to fit the spectral energy distribution of dust using a model to separate the effects of dust properties, dust temperature and column density. The dust emission in the SPIRE wavelength range is dominated by big grains at thermal equilibrium with the ambient radiation field. It is often modelled as a modified black body spectrum:

$$I_{\nu} = \tau_{\nu_0} B_{\nu}(T_{\text{obs}}) \left(\frac{\nu}{\nu_0} \right)^{\beta_{\text{obs}}} \quad (\text{A.1})$$

where τ_{ν_0} is the optical depth at a reference frequency ν_0 , T_{obs} represents the dust equilibrium temperature and β_{obs} the dust spectral index. For a constant dust emissivity and a constant dust-to-gas ratio, τ_{ν_0} is proportional to gas column density. It can thus be used as a tracer of the structure of matter projected on the sky.

To obtain τ_{ν_0} it is common practice to fit the dust emission pixel by pixel, by combining PACS and SPIRE data for instance. This is unfortunately impossible in our case because of the failure of the PACS observations.

A similar fit has been performed over the whole sky by Planck Collaboration et al. (2014a) using *IRAS* 100 μm data and *Planck* 350, 550 and 850 μm data. The maps of $\tau_{353\text{GHz}}$, T_{obs} and β_{obs} for the Draco field are shown in Fig. A.1. These maps have an angular resolution of $5'$, $5'$ and $30'$ respectively. As a comparison, the SPIRE 250 μm map convolved at $5'$ is also shown in Fig. A.1. The morphological resemblance of $I_{250\mu\text{m}}$ and $\tau_{353\text{GHz}}$ is striking, indicating that variations of dust properties and dust temperature are not dominating the observed emission fluctuations in the SPIRE bands. This is confirmed by looking at the maps of T_{obs} and β_{obs} computed by Planck Collaboration et al. (2014a). The 1σ variations of T_{obs} and β_{obs} are only 3% and the structure of Draco is barely visible in these parameter maps. This is in accordance with the fact that there are no local sources of heating photons and a relatively low extinction; locally the radiation field appears to be very uniform.

In addition we note the presence of small scale structure in T_{obs} , apparently unrelated to variations of the dust equilibrium temperature. These fluctuations were observed and quantified by Planck Collaboration et al. (2014a); they are caused by the Cosmic Infrared Background anisotropies (CIBA). In such a diffuse high Galactic latitude field, the CIBA appear quite strongly in the map of T_{obs} (see Planck Collaboration et al. (2014a) for details).

Even though the *Planck* dust products are at significantly lower resolution than the SPIRE data, one could envisage estimating the dust column density by correcting for T_{obs} and β_{obs} obtained with *Planck*. We conclude that the variations in T_{obs} that would be of interstellar origin are not strong enough to overcome the drawback of affecting the data with the CIBA. In addition the correlation of $I_{250\mu\text{m}}$, convolved at $5'$, with $\tau_{353\text{GHz}}$ is extremely tight (see Fig. A.2), with residuals compatible with CIBA.⁵ For those reasons we decided to simply multiply $I_{250\mu\text{m}}$ by a single factor to translate it to hydrogen column density, N_{H} . To do so, we use the $I_{250\mu\text{m}}-\tau_{353\text{GHz}}$ correlation shown in Fig. A.2 combined with the relationship $\tau_{353\text{GHz}} = 6.3 \times 10^{-27} N_{\text{HI}}$ that Planck Collaboration et al. (2014a) found by comparing *Planck* and 21 cm data at high Galactic latitude. This leads to the following relation:

$$N_{\text{H}} = 2.49 \times 10^{20} I_{250\mu\text{m}} \quad (\text{A.2})$$

where $I_{250\mu\text{m}}$ is the zero level corrected map, expressed in MJy sr^{-1} , and N_{H} is the total hydrogen column density (H I and H₂) expressed in cm^{-2} . Because we assumed constant values for T_{obs} and β_{obs} , no color correction is needed in the correspondence between $I_{250\mu\text{m}}$, $\tau_{353\text{GHz}}$ and N_{H} .

Appendix B: Terminal velocity

Following Benjamin & Danly (1997), a cloud falling in the halo of a Galaxy will reach a terminal velocity that depends on its Galactic height, z , its column density, N_{H} , the gravitational acceleration of the galaxy, $g(z)$, the density distribution of the gas, $n(z)$, and on a parameter that quantify the efficiency of the friction, C_d :

$$v_t(z) = \sqrt{\frac{2 N_{\text{H}} g(z)}{C_d n(z)}}. \quad (\text{B.1})$$

⁵ the linear relation shown in Fig. A.2 was used to set the zero level of the SPIRE map

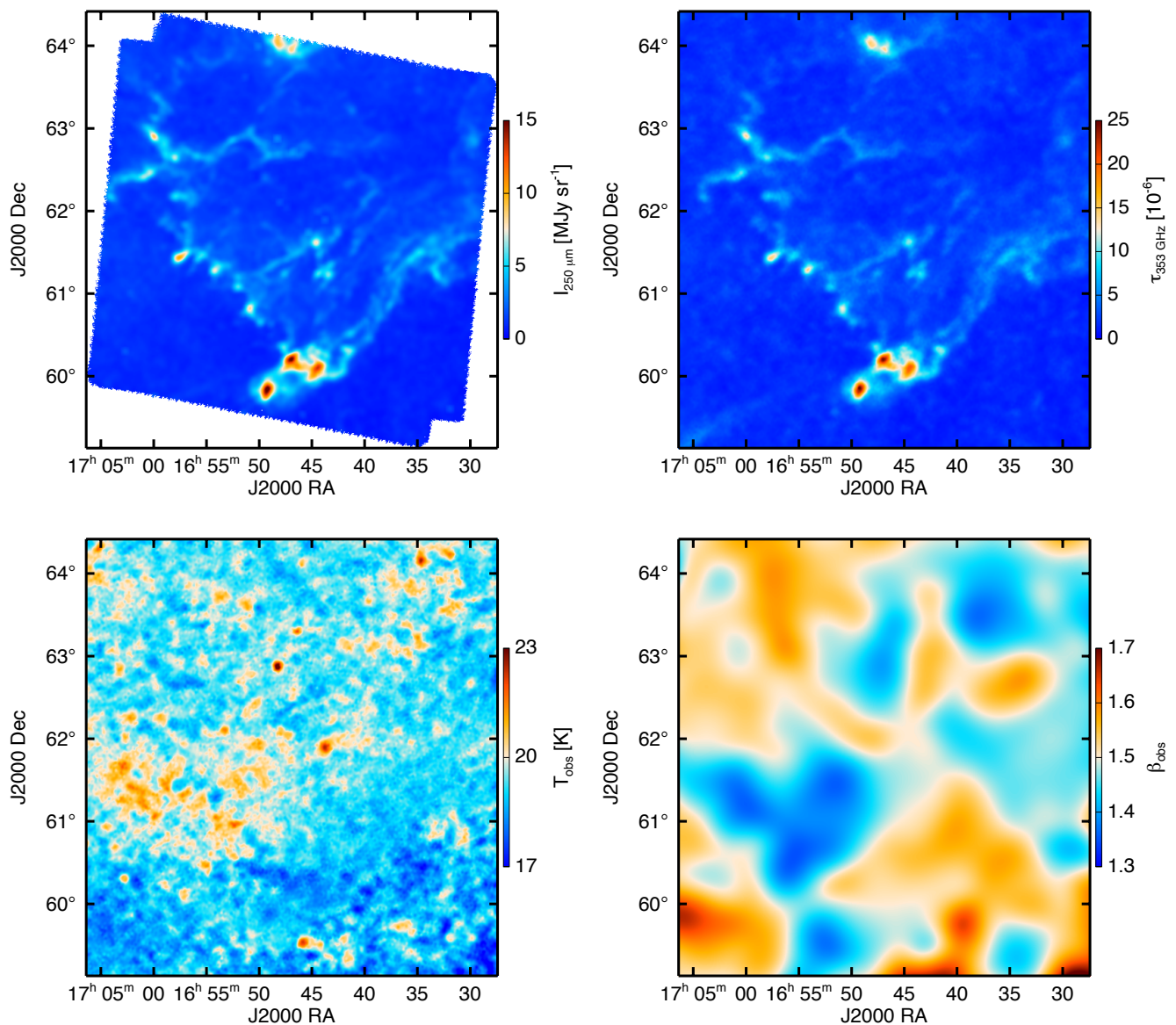


Fig. A.1: Comparison of *Herschel*-SPIRE and *Planck* data of Draco. *Herschel*-SPIRE at $250\ \mu\text{m}$ (top left), *Planck* τ_{353} (top right), *Planck* T_{obs} (bottom left), and *Planck* β_{obs} (bottom right). All maps have an angular resolution of $5'$ except β_{obs} that is at $30'$.

For $g(z)$ and $n(z)$, we used the prescription of Benjamin & Danly (1997). The total gravitational acceleration (gas and stars) is approximated by

$$g(z) = 9.5 \times 10^{-9} \tanh(z/400\text{pc}). \quad (\text{B.2})$$

The gas distribution is the sum of the H I layer (Dickey & Lockman 1990), the WIM layer (Reynolds 1993) and of a hot ionized layer (Wolfire et al. 1995) (for details, see Benjamin & Danly 1997).

The column density of Draco is estimated to be $N_{\text{H}} = 1.3 \times 10^{20} \text{ cm}^{-2}$. Like in (Benjamin & Danly 1997), we assumed $C_{\text{d}} = 1$.

In this context, a cloud entering the disk is slowed down by the friction with the ISM. The deceleration can be estimated by

$$a_{\text{t}} = v_{\text{t}} \frac{dv_{\text{t}}}{dz}. \quad (\text{B.3})$$

Figure B.1 shows the terminal velocity and the deceleration curves for a cloud with $N_{\text{H}} = 1.3 \times 10^{20} \text{ cm}^{-2}$. The bottom plot of Fig. B.1 shows the density profile of the H I, WIM and HIM.

References

- Audit, E. & Hennebelle, P. 2005, *A&A*, 433, 1
 Audit, E. & Hennebelle, P. 2010, *A&A*, 511, A76
 Beck, R. 2001, *Space Sci. Rev.*, 99, 243
 Benjamin, R. 1999, in *Interstellar Turbulence*, ed. J. Franco & A. Carraminana, 49
 Benjamin, R. A. & Danly, L. 1997, *ApJ*, 481, 764
 Blagrave, K., Martin, P. G., Joncas, G., et al. 2016, *ArXiv e-prints*
 Bregman, J. N. 1980, *ApJ*, 236, 577
 Burrows, D. N. & Mendenhall, J. A. 1991, *Nature*, 351, 629
 Chandrasekhar, S. 1949, *ApJ*, 110, 329
 Chandrasekhar, S. 1961, *Hydrodynamic and hydromagnetic stability*
 Collins, J. A., Shull, J. M., & Giroux, M. L. 2007, *ApJ*, 657, 271
 Dickey, J. M. & Lockman, F. J. 1990, *ARA&A*, 28, 215
 Ellinger, C. I., Young, P. A., Fryer, C. L., & Rockefeller, G. 2012, *ApJ*, 755, 160
 Federrath, C., Klessen, R. S., & Schmidt, W. 2009, *ApJ*, 692, 364

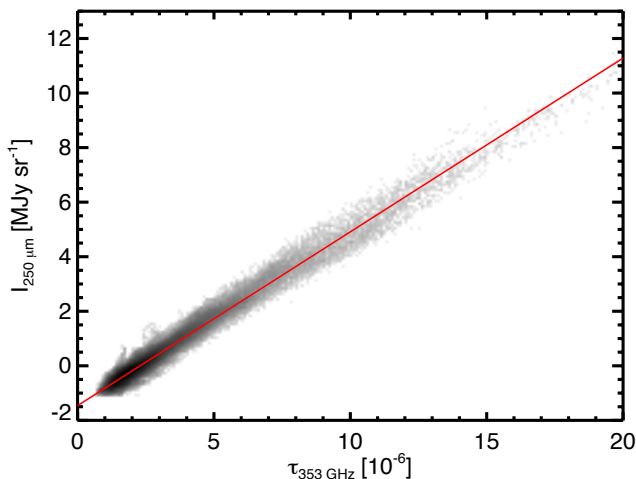


Fig. A.2: *Herschel*-SPIRE 250 μm intensity, smoothed to 5', compared to *Planck* optical depth at 353 GHz. The red line is the linear relation $I_{250\mu\text{m}} = 6.37 \times 10^5 \tau_{353\text{GHz}} - 1.46$. The intercept of this relation was removed from the $I_{250\mu\text{m}}$ map to set its zero level.

Gladders, M. D., Clarke, T. E., Burns, C. R., et al. 1998, *ApJ*, 507, L161
 Goerigk, W. & Mebold, U. 1986, *A&A*, 162, 279
 Goerigk, W., Mebold, U., Reif, K., Kalberla, P. M. W., & Velden, L. 1983, *A&A*, 120, 63
 Griffin, M. J., Abergel, A., Abreu, A., et al. 2010, *A&A*, 518, L3
 Heithausen, A., Bensch, F., Stutzki, J., Falgarone, E., & Panis, J. F. 1998, *A&A*, 331, L65
 Heitsch, F. & Putman, M. E. 2009, *ApJ*, 698, 1485
 Hennebelle, P. & André, P. 2013, *A&A*, 560, A68
 Hennebelle, P., Audit, E., & Miville-Deschênes, M.-A. 2007, *A&A*, 465, 445
 Hennebelle, P. & Falgarone, E. 2012, *A&A Rev.*, 20, 55
 Hennebelle, P. & Pérault, M. 1999, *A&A*, 351, 309
 Herbstmeier, U., Heithausen, A., & Mebold, U. 1993, *A&A*, 272, 514
 Herbstmeier, U., Moritz, P., & Heithausen, A. 1994, in *The First Symposium on the Infrared Cirrus and Diffuse Interstellar Clouds*, ed. R. M. Cutri & W. B. Latter, Vol. 58, 176
 Heyer, M., Krawczyk, C., Duval, J., & Jackson, J. M. 2009, *ApJ*, 699, 1092
 Heyer, M. H., Carpenter, J. M., & Snell, R. L. 2001, *ApJ*, 551, 852
 Hirth, W., Mebold, U., & Mueller, P. 1985, *A&A*, 153, 249
 Inoue, T. & Inutsuka, S.-i. 2009, *ApJ*, 704, 161
 Joung, M. R., Bryan, G. L., & Putman, M. E. 2012, *ApJ*, 745, 148
 Kalberla, P. M. W., Mebold, U., & Reif, K. 1982, *A&A*, 106, 190
 Kalberla, P. M. W., Herbstmeier, U., & Mebold, U. 1984, in *NASA Conference Publication*, ed. Y. Kondo, F. C. Bruhweiler, & B. D. Savage, Vol. 2345, 243
 Kerp, J., Burton, W. B., Egger, R., et al. 1999, *A&A*, 342, 213
 Könyves, V., André, P., Men'shchikov, A., et al. 2010, *A&A*, 518, L106
 Koyama, H. & Inutsuka, S.-I. 2000, *ApJ*, 532, 980
 Kramer, C., Stutzki, J., Rohrig, R., & Corneliussen, U. 1998, *A&A*, 329, 249
 Kritsuk, A. G., Norman, M. L., Padoan, P., & Wagner, R. 2007, *ApJ*, 665, 416
 Lequeux, J. 2005, *The Interstellar Medium (CNRS Édition)*
 Lilienthal, D., Wennmacher, A., Herbstmeier, U., & Mebold, U. 1991, *A&A*, 250, 150
 Magnani, L., Blitz, L., & Mundy, L. 1985, *ApJ*, 295, 402
 Magnani, L. & Smith, A. J. 2010, *ApJ*, 722, 1685
 Marshall, D. J., Joncas, G., & Jones, A. P. 2009, *ApJ*, 706, 727
 Martin, P. G., Blagrove, K. P. M., Lockman, F. J., et al. 2015, *ApJ*, 809, 153
 Mebold, U., Cernicharo, J., Velden, L., et al. 1985, *A&A*, 151, 427
 Mebold, U., Herbstmeier, U., Kalberla, P. M. W., & Souvatzis, I. 1989, in *IAU Colloq. 120: Structure and Dynamics of the Interstellar Medium*, ed. G. Tenorio-Tagle, M. Moles, & J. Melnick, Vol. 350, 424
 Meisner, A. M. & Finkbeiner, D. P. 2014, *ApJ*, 781, 5
 Moritz, P., Wennmacher, A., Herbstmeier, U., et al. 1998, *A&A*, 336, 682
 Odenwald, S. F. & Rickard, L. J. 1987, *ApJ*, 318, 702
 Park, S.-J., Min, K.-W., Seon, K.-I., et al. 2009, *ApJ*, 700, 155
 Peek, J. E. G., Putman, M. E., & Sommer-Larsen, J. 2008, *ApJ*, 674, 227
 Penprase, B. E., Rhodes, J. D., & Harris, E. L. 2000, *A&A*, 364, 712
 Pietz, J., Kerp, J., Kalberla, P. M. W., et al. 1996, *A&A*, 308, L37
 Planck Collaboration, Abergel, A., Ade, P. A. R., et al. 2014a, *A&A*, 571, A11
 Planck Collaboration, Abergel, A., Ade, P. A. R., et al. 2011, *A&A*, 536, A24
 Planck Collaboration, Ade, P. A. R., Aghanim, N., et al. 2014b, *A&A*, 571, A13

Putman, M. E., Peek, J. E. G., & Joung, M. R. 2012, *ARA&A*, 50, 491
 Reynolds, R. J. 1993, in *Back To The Galaxy*, ed. S. S. Holt & F. Verter (New York: AIP conference proceedings), 156
 Ribeyre, X., Tikhonchuk, V. T., & Bouquet, S. 2004, *Physics of Fluids*, 16, 4661
 Rohlfs, R., Herbstmeier, U., Mebold, U., & Winnberg, A. 1989, *A&A*, 211, 402
 Roman-Duval, J., Jackson, J. M., Heyer, M., Rathborne, J., & Simon, R. 2010, *apj*, 723, 492
 Sancisi, R., Fraternali, F., Oosterloo, T., & van der Hulst, T. 2008, *A&A Rev.*, 15, 189
 Saury, E., Miville-Deschênes, M.-A., Hennebelle, P., Audit, E., & Schmidt, W. 2014, *A&A*, 567, A16
 Shapiro, P. R. & Field, G. B. 1976, *ApJ*, 205, 762
 Snowden, S. L., Mebold, U., Hirth, W., Herbstmeier, U., & Schmitt, J. H. M. 1991, *Science*, 252, 1529
 Solomon, P. M., Rivolo, A. R., Barrett, J., & Yahil, A. 1987, *ApJ*, 319, 730
 Stark, R., Kalberla, P., & Guesten, R. 1997, *A&A*, 317, 907
 Vázquez-Semadeni, E., Ryu, D., Passot, T., González, R. F., & Gazol, A. 2006, *ApJ*, 643, 245
 Wardle, M. 1990, *MNRAS*, 246, 98
 Williams, J. P., de Geus, E. J., & Blitz, L. 1994, *ApJ*, 428, 693
 Wolfire, M. G., McKee, C. F., Hollenbach, D., & Tielens, A. G. G. M. 1995, *ApJ*, 453, 673

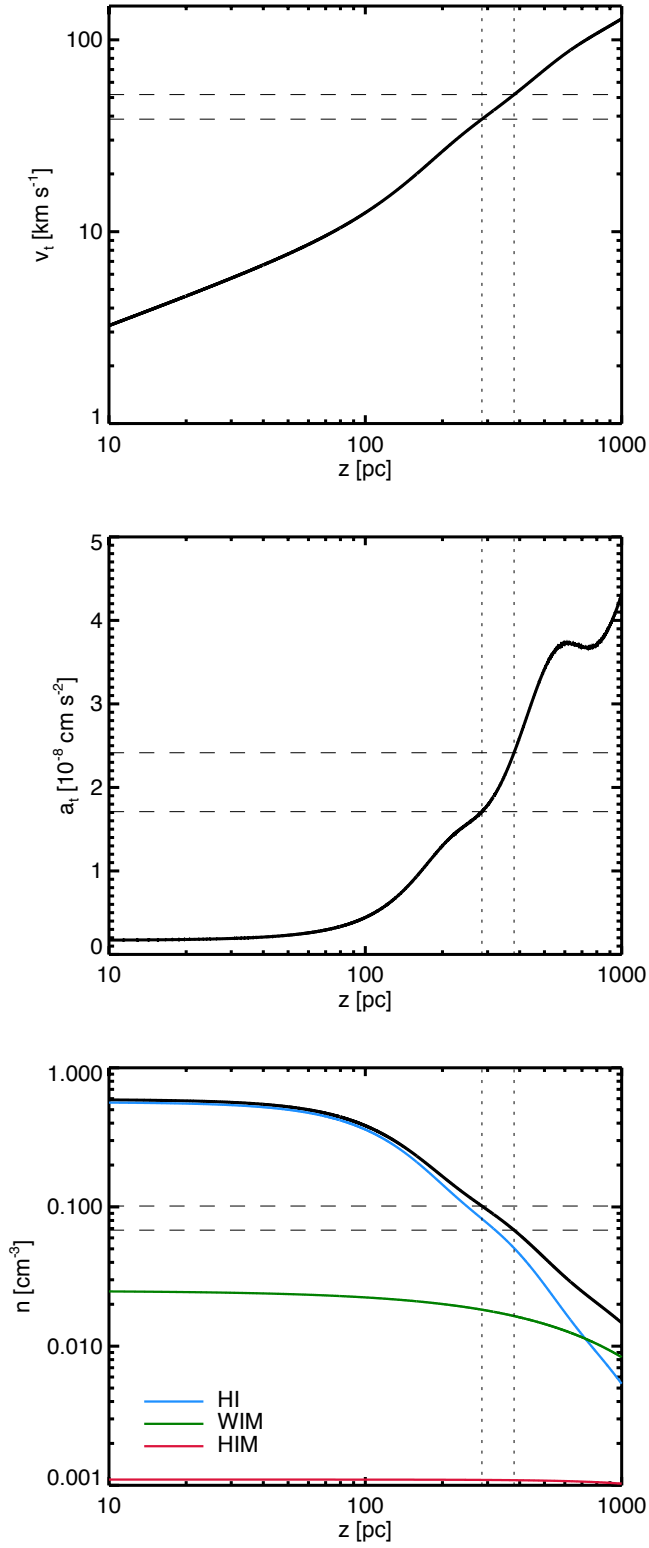


Fig. B.1: Terminal velocity (top) and deceleration (middle) as a function of Galactic height for a cloud of $N_{\text{H}} = 1.3 \times 10^{20} \text{ cm}^{-2}$. The bottom panel is the gas density vs z , including the H I, the WIM and the HIM. The dotted lines indicate the range in distance of Gladders et al. (1998) and the dashed lines show the corresponding values on each curve.